

Nature of the Soft Spectral Component in the X-ray Pulsars SMC X-1 and LMC X-4

B. Paul^{1,2}, F. Nagase¹, T. Endo¹, T. Dotani¹, J. Yokogawa³, and M. Nishiuchi³

ABSTRACT

We present here the results of an investigation of the pulse averaged and pulse phase resolved energy spectra of two high luminosity accretion powered X-ray pulsars SMC X-1 and LMC X-4 made with ASCA. The phase averaged energy spectra definitely show the presence of a soft excess in both the sources. If the soft excess is modeled as a separate black-body or thermal bremsstrahlung type component, pulse phase resolved spectroscopy of SMC X-1 shows that the soft component also has a pulsating nature. Same may be true for LMC X-4, though a very small pulse fraction limits the statistical significance. The pulsating soft component is found to have a nearly sinusoidal profile, dissimilar to the complex profile seen at higher energies, which can be an effect of smearing. Due to very high luminosity of these sources, the size of the emission zone required for the soft component is large (radius $\sim 300\text{--}400$ km). We show that the pulsating nature of the soft component is difficult to explain if a thermal origin is assumed for it. We further investigated with alternate models, like inversely broken power-law or two different power-law components and found that these models can also be used to explain the excess at low energy. A soft power-law component may be a common feature of the accreting X-ray pulsars, which is difficult to detect because most of the HMXB pulsars are in the Galactic plane and experience large interstellar absorption. In LMC X-4, we have also measured two additional mid-eclipse times, which confirm the known orbital decay.

Subject headings: stars : neutron — Pulsars : individual (LMC X-4, SMC X-1)
— X-rays : stars

¹The Institute of Space and Astronautical Science, 3-1-1 Yoshinodai, Sagamihara, Kanagawa 229-8510, Japan, nagase@astro.isas.ac.jp, dotani@astro.isas.ac.jp, etakao@isl.melco.co.jp

²Tata Institute of Fundamental Research, Homi Bhabha road, Mumbai, 400 005, India bpaul@tifr.res.in

³Department of Physics, Graduate School of Science, Kyoto University, Sakyo-ku, Kyoto, 606-8502, Japan jun@cr.sphys.kyoto-u.ac.jp, nishiuchi@apr.jaeri.go.jp

1. Introduction

The X-ray continuum spectra of accreting pulsars are often described as a broken power-law or a power-law with exponential cutoff. The break in the spectrum is in the range of 10–20 keV and power-law photon index below the break energy is in the range of 0–1 (White, Nagase & Parmar 1995). Some binary X-ray pulsars which are away from the Galactic plane and therefore experience less interstellar absorption, show the presence of a soft component in the spectrum which is often modeled as a black-body and/or thermal bremsstrahlung emission (SMC X-1: Marshall, White, & Becker 1983; Woo et al. 1995; Wojdowski et al. 1998; LMC X-4: Dennerl 1989; Woo et al. 1996; RX J0059.2–7138: Kohno, Yokogawa, & Koyama 2000; 4U 1626–67: Orlandini et al. 1998; Her X-1: McCray et al. 1982, Dal Fiume et al. 1998; Oosterbroek et al. 1997, 2000; Endo, Nagase & Mihara 2000) or an inversely broken power-law (XTE J0111.2–7317: Yokogawa et al. 2000b). The soft component in 4U 1626–67, when modeled as a black-body emission requires the size of emission region to be comparable to that of the neutron star because the intrinsic luminosity of this source is of the order of 10^{35} erg s⁻¹ (Orlandini et al. 1998). On the other hand, the soft component in Her X-1 can be modeled as a black-body which is reprocessed emission from the innermost part of the accretion disk (Endo et al. 2000). However, for the bright pulsars in the Magellanic Clouds for which the distance is of the order of 50–60 kpc and the luminosity is close to the Eddington limit, the luminosity of the soft excess is about an order of magnitude larger compared to the same of Her X-1. Therefore, a pulsating nature of the soft component that has been observed in some high luminosity X-ray pulsars (LMC X-4 : Woo et al. 1996 and XTE J0111.2–7317 : Yokogawa et al. 2000b) needs to be probed with greater detail.

To investigate the pulse phase dependence of the soft component of accreting X-ray pulsars in detail, we have chosen two luminous X-ray pulsars SMC X-1 and LMC X-4, which are in the Magellanic Clouds and suffer less interstellar absorption. SMC X-1 and LMC X-4 are two bright, eclipsing, accreting, binary X-ray pulsars with spin periods of ~ 0.7 and ~ 13.5 s and binary periods of ~ 3.9 and ~ 1.4 day respectively. The companion of SMC X-1 is a B0 supergiant while the companion star of LMC X-4 is of type O7III-V. The binary orbits of both the systems are nearly circular. The orbital period of the two binaries are found to decay with time scale of 3×10^5 yr in SMC X-1 (Wojdowski et al. 1998), and 10^6 yr in LMC X-4 (Levine, Rappaport & Zojcheski 2000). Another striking similarity between these two sources is a long-period of 50–60 day and 30.5 day respectively, that is known to be quasi-stable in SMC X-1 (Wojdowski et al. 1998) and stable in LMC X-4 (Lang et al. 1981). The long-period is believed to be a result of (quasi) periodic obscuration of the neutron star by a precessing accretion disk, similar to that in Her X-1. Broad band energy-spectra (0.2–37 keV) of these two sources were studied by performing a combined fit to the observations made with ROSAT and GINGA (Woo et al. 1995; 1996). In addition to a cutoff power-law type

component in SMC X-1 (photon index of ~ 0.93 , $E_C = 5.6$ keV, $E_F = 15$ keV) and power-law type component in LMC X-4 (photon index of ~ 0.67) broad iron emission lines and soft excess were detected. The soft component was modeled as a single black-body component ($kT_{\text{BB}} = 0.16$ keV) in SMC X-1 and as a sum of a low temperature black-body emission ($kT_{\text{BB}} = 0.03$ keV) and a thermal bremsstrahlung emission ($kT_{\text{TB}} = 0.35$ keV) in LMC X-4. Beppo-SAX observations also showed presence of similar soft component (La Barbera et al. 2001). From HEAO-1 observations, the soft X-rays from SMC X-1 were found to be nonpulsating (Marshall et al. 1983). However, the ROSAT and ASCA observations detected clear pulsations with a pulse profile different from the hard component (Wojdowski et al. 1998). Pulse phase resolved spectroscopy of combined ROSAT and GINGA data of LMC X-4 revealed modulation of the thermal bremsstrahlung and iron line emission components with pulse phase (Woo et al. 1996).

We note that the combined fit of the ROSAT and GINGA spectra of these two sources were performed on non-simultaneous observations and the intensity and spectral shape of these sources are known to be variable. We have carried out pulse phase averaged and pulse phase resolved spectral studies in the 0.5–10.0 keV band. In this paper we present the results of our investigation to the nature of the soft excess through pulse profiles in different energy bands and variations of the different spectral components with pulse phase.

2. Observations

The observations of SMC X-1 and LMC X-4, presented here were made with the Advanced Satellite for Cosmology and Astrophysics (ASCA). ASCA is equipped with two Solid-state Imaging Spectrometers (SIS) and Gas Imaging Spectrometers (GIS), each at the focal plane of four identical mirrors of typical photon collecting area ~ 150 cm² at 6 keV. The energy resolution is 130 and 500 eV (FWHM) at 6 keV for the SIS and GIS detectors respectively. For more details about ASCA refer to Tanaka, Inoue & Holt (1994).

SMC X-1 was observed twice with ASCA during 1993 April 16–27, and 1995 October 18–19, and it was at the edge of the GIS field of view in an observation of XTE 0111.2–7317 made during 1998 November 18–19 (Yokogawa et al. 2000a; 2000b). The first observation was in the high state of its long-period intensity variation of 50–60 day, while the second one was in the low state. Results from timing, and some spectral analysis of these observations were presented by Wojdowski et al. (1998) and Yokogawa et al. (2000a). For the present study, we have selected the first observation made in 1993 which has the best photon statistics. In this observation, the GIS detectors were operated in normal PH mode with time resolution of 1.953 ms and 15.625 ms for high and medium bit-rate, respectively, while the SIS observations

were made with one of the CCD chips, with time resolution of 4 s. Out of eclipse data obtained during the first 60 ks of the observation resulted into 20.5 ks and 18 ks of useful data with each of the GIS and SIS detectors respectively. The GIS and SIS spectra have been used for phase averaged spectroscopy while for phase resolved studies only data from GIS could be used. Wojdowski et al. (1998) determined the pulse periods and other orbital parameters of SMC X-1 from the ASCA observations.

LMC X-4 was observed with ASCA on three occasions, 1994 April 26–27, 1995 November 24–25, and 1996 May 24–25, all during the high state of its 30.5 day long-period. The second observation was carried out mainly during the eclipse. Of the remaining two, we have selected the third observation for the present study, because there were some dips in the first observation with associated spectral changes which makes the analysis more complicated. For analysis of the orbital period decay in LMC X-4, however, both the 1994 and 1996 observations were used. Some preliminary results from some of these observations were reported by Vrtilik et al. (1997). In the 1996 observation, the GIS detectors were operated in normal PH mode in which the time resolution is 62.5 ms and 500 ms at high and medium bit rates respectively. Total exposure of 36 ks was obtained with the GIS, of which 31 ks of observation is outside the eclipse. Observations with the SIS detectors were made with one of the CCD chips. SIS0 was operated in FAST mode with time resolution of 15.625 ms while SIS1 was operated in BRIGHT (imaging) mode which has a time resolution of 4 s. The average total exposure and out of eclipse exposure with the two SIS detectors were 33.5 ks and 28.5 ks respectively. The GIS and SIS1 data outside the eclipse have been used for phase averaged spectroscopy while GIS data obtained only in the high bit rate and SIS0 FAST mode data have been used for timing and pulse phase resolved spectroscopy. The pulse periods of LMC X-4 obtained from these ASCA observations have been reported by Vrtilik et al. (1997).

3. Analysis and results

We used the standard data selection criteria of the ASCA guest observer facility. Data from the hot and flickering pixels of the SIS detectors were removed. Charged particle events were removed from the GIS data based on the rise time discrimination method. The count rates and spectra of the source were obtained from circular regions of radius $6'$ for the GIS detectors and $4'$ for the SIS detectors. For SIS, the background spectra were extracted from the whole chip excluding a circular region around the source and for GIS it was collected from regions diametrically opposite to the source location in the field of view.

3.1. SMC X-1

3.1.1. Pulse profile

This observation was made in 1993 April 16–27. Near the end of this observation, the source went into an eclipse and the count rate shows a gradual decrease. The light curve obtained from this observation is shown in Figure 1 for different energy bands. In the present work, we have used data only from the first 60 ks when the source was out of eclipse and the count rate was high.

To create the pulse profiles, and to carry out pulse phase resolved spectroscopy, the photon arrival times were reassigned after solar system barycenter correction and correction for the arrival time delays due to orbital motion. The orbital parameters and the pulse period were taken from Wojdowski et al. (1998). The pulse profile, shown in Figure 2, is single peaked at energies < 1.0 keV, with an additional small peak at higher energies. The pulse phases are identical in different energy bands. The pulse fraction is somewhat larger at higher energies.

3.1.2. Phase averaged spectrum

After appropriate background subtraction, pulse phase averaged spectra from the pairs of GIS and SIS detectors were combined and were fitted simultaneously. The relative normalisation of the SIS detectors was allowed to vary and all the other spectral parameters were tied to be the same for SIS and GIS. The energy ranges chosen for spectral fitting are 0.55–10.0 keV for the SIS and 0.7–10.0 keV for the GIS. All the spectral analysis reported in this paper were carried out using the spectral analysis package XSPEC.

The spectra, in addition to a hard power-law component with photon index ~ 0.9 , also showed iron line and soft excess. We found that to explain the soft excess, a second component is needed. The soft excess can be fitted to either a (a) black-body, (b) bremsstrahlung, (c) soft power-law, or (d) inversely broken power-law. We found that a partial covering model does not fit the spectrum well. In SMC X-1, the hard power-law component is known to have an exponential cutoff at 6 keV with a e -folding energy of ~ 25 keV (Woo et al. 1996). This was also found in the ASCA data and a high energy exponential cutoff component was included. Analytic form of the different models used are as follows:

$$\begin{aligned} \text{Model I} : f(E) &= e^{-\sigma(E)N_{\text{H}}} (f_{\text{PF}}(E) + f_{\text{PL}}(E)f_{\text{cut}}(E) + f_{\text{Fe}}(E)), \\ \text{Model II} : f(E) &= e^{-\sigma(E)N_{\text{H}}} (f_{\text{TB}}(E) + f_{\text{PL}}(E)f_{\text{cut}}(E) + f_{\text{Fe}}(E)), \\ \text{Model III} : f(E) &= e^{-\sigma(E)N_{\text{H}}} (f_{\text{PLBKN}}(E)f_{\text{cut}}(E) + f_{\text{Fe}}(E)), \end{aligned}$$

$$\begin{aligned}
 \text{Model IV : } f(E) &= e^{-\sigma(E)N_{\text{H}}} (f_{\text{PLS}}(E) + f_{\text{PL}}(E)f_{\text{cut}}(E) + f_{\text{Fe}}(E)), \\
 f_{\text{PF}}(E) &= \frac{I_{\text{PF}} \left(\frac{E}{kT_{\text{PF}}}\right)^2 (e - 1)}{e^{\frac{E}{kT_{\text{PF}}}} - 1}, \quad f_{\text{TB}}(E) = I_{\text{TB}} \frac{G(E, kT_{\text{TB}})}{E} e^{-\frac{E}{kT_{\text{TB}}}}, \\
 f_{\text{PL}}(E) &= I_{\text{PL}} E^{-\Gamma_1}, \quad f_{\text{PLS}}(E) = I_{\text{PLS}} E^{-\Gamma_2}, \\
 f_{\text{PLBKN}}(E) &= \left\{ \begin{array}{l} I_{\text{P}} E^{-\Gamma_2} \quad (E < E_{\text{b}}) \\ I_{\text{P}} E_{\text{b}}^{(\Gamma_1 - \Gamma_2)} E^{-\Gamma_1} \quad (E \geq E_{\text{b}}; \Gamma_1 < \Gamma_2) \end{array} \right\}, \\
 f_{\text{cut}}(E) &= \left\{ \begin{array}{l} 1 \quad (E < E_{\text{C}}) \\ e^{-\frac{E - E_{\text{C}}}{E_{\text{F}}}} \quad (E \geq E_{\text{C}}) \end{array} \right\}, \\
 f_{\text{Fe}}(E) &= \frac{I_{\text{Fe}}}{\sqrt{2\pi\sigma_{\text{Fe}}^2}} \exp\left[-\frac{(E - E_{\text{Fe}})^2}{2\sigma_{\text{Fe}}^2}\right],
 \end{aligned}$$

where E is the incident photon energy, $\sigma(E)$ is the photo-electric absorption cross-section (Morrison & McCammon 1983), $G(E, kT_{\text{TB}})$ is the Gaunt factor at energy E for a plasma of temperature kT_{TB} keV. E_{C} and E_{F} are the cutoff energy and the e -folding energy respectively.

The phase averaged spectrum could be fitted well with all the four models and the parameters obtained for each model are given in Table 1. The photon index (Γ_1) of the hard power-law component is identical in all the four models, ~ 0.9 . The cutoff energy is found to be 5.5 keV and the e -folding energy above the cut-off is 25 keV. In SMC X-1, a black-body type model for the soft component requires a temperature of 0.18 keV and for a distance of 65 kpc of the SMC, it should have a radius of ~ 400 km. The SIS and GIS count rate spectra of SMC X-1 are shown in Figure 3 along with the components of model-I and the residuals. A thermal bremsstrahlung type emission for the soft excess requires a temperature of 0.33 keV and emission measure of $7 \times 10^{61} \text{ cm}^{-3}$. In case of an additional power-law, it has a photon index of 4.8, whereas in inversely broken power-law model, the soft photon index is ~ 1.9 and the break energy is ~ 1.7 keV. The iron K_{α} line has an equivalent width of 120 ± 30 eV and it is found to be broad (gaussian $\sigma = 0.5$ keV).

3.1.3. Pulse phase resolved spectrum

To extract the phase resolved spectra, phase filtering was applied within the FTOOLS task XSELECT. In this method, the photon arrival time or the center time of each data bin is used to determine which phase bin the photon belongs to. In order to search for variability of the soft component, the phase resolved spectra were fitted with the models I and II which have a thermal component for the soft excess. A pulsating nature of the soft

component has been detected in both the models with identical amplitude. Here we discuss only the results obtained with the first model. At first we created four phase resolved spectra consisting the main pulse, sub pulse, and two minima of the pulse profile as shown in the bottom panel of Figure 2. While fitting these four spectra, all the spectral parameters were allowed to vary. The results of this analysis are shown in Figure 4 and Table 2. While the normalisation of the power-law and black-body components are found to have considerable variation (Table 2), variations of the black-body temperature and photon index are within measurement uncertainties. Since we have used GIS data in the energy range 0.7-10.0 keV, the column density values are not well constrained to see any measurable variation (Table 2). We, therefore, fixed most of the spectral parameters to their phase averaged value during the later part of the phase resolved spectroscopy, when we have more phase bins and poorer statistics in each phase bin.

Further, 16 pulse phase resolved spectra were obtained only from the GIS data. The variations of the power-law flux, black-body flux, and the total flux with the pulse phase are shown in Figure 5. It is clearly seen that the strength of the power-law component has a profile similar to the pulse profile. The black-body component shows a nearly sinusoidal intensity variation with the pulse phase. There is also phase difference between the soft and hard pulse profiles. A constant fit to the phase resolved black-body flux gives a reduced χ^2 of 7.2 and a sinusoidal fit improves the reduced χ^2 to 4.0. While a sinusoidal does not represent the variation of the black-body flux very well, poorness of the first fit certainly shows a varying nature of the black-body flux.

Assuming that the pulse profiles at different narrow energy bands are made of two components, one nearly sinusoidal and the other complex (shown in the top and middle panels of Figure 5), we have estimated the fraction of sinusoidal and complex components in the SMC X-1 pulse profile at different energies. The narrow band pulse profiles were fitted to a composite of two templates (made from the top and middle panels of Figure 5) and the fractions of the two components that give minimum χ^2 was found out. In Figure 6, we compare this with the ratio of the black-body to total flux derived from the best fit spectral model. A reasonable agreement between the two provides a consistency for the hypothesis that there are two spectral components with different pulse profiles.

3.2. LMC X-4

3.2.1. *Orbital period decay*

The orbital period of LMC X-4 is known to have a decay time scale of 10^6 yr. The decay rate of the binary orbit of LMC X-4 has been established with high confidence by combining the earlier known mid-eclipse times with a recent precise measurement with the RXTE (Levine et al. 2000). From the ASCA observations of LMC X-4, we have determined two more mid-eclipse times. Among the four orbital parameters, orbital period, semi-amplitude of the arrival time delay, eccentricity and mid-eclipse time, the later is likely to have maximum variation between observation to observation. This also allows precise measurement of the period change. A small pulse fraction and low count rate of LMC X-4 with ASCA, does not allow us to directly apply the pulse arrival time analysis. We, therefore adopted a different approach to determine the mid-eclipse time.

After the barycentric corrections, the light curves were corrected for delays due to the orbital motion with the known semi-amplitude, orbital period and zero eccentricity of the system for various trial mid-eclipse times around its extrapolated value. The epoch-folding technique was applied on each of these light curves (with time resolution of 62.5 ms) and the maximum χ^2 and the pulse period corresponding to each trial mid-eclipse time was determined. The distribution of maximum χ^2 against the trial mid-eclipse times are shown in Figure 7 for the two ASCA observations in 1994 and 1996. The maximum χ^2 distribution has a gaussian profile around its expected value, the center of which gives the correct mid-eclipse time. The two mid eclipse times obtained are $\text{MJD } 49468.6859 \pm 0.0054$ and $\text{MJD } 50227.8069 \pm 0.0016$ and the corresponding pulse periods are 13.5075 ± 0.0002 s and 13.5088 ± 0.0001 s respectively. In absence of a clear method of error determination, we have taken the width of the gaussians as the error of the mid-eclipse time, which possibly is an overestiamtion.

The mid-eclipse times determined here are consistent with the orbital evolution history of LMC X-4 with evolution time scale of 10^6 yr (Levine et al. 2000). The pulse profiles obtained from the GIS detectors are shown in Figure 8 for two different and summed energy bands. The profile is a single peaked sinusoidal in the low energy band of 0.5–1.5 keV and is complex with multiple peaks in the higher energy band of 1.5–10.0 keV. For pulse phase resolved spectroscopy, orbital motion of the neutron star was corrected in the light curve using the known semi-amplitude, eccentricity (Levine et al. 2000) and mid-eclipse time derived from the ASCA data.

3.2.2. Phase averaged spectrum

The four spectral models used for fitting the SMC X-1 spectrum were modified slightly for the LMC X-4 spectrum. The high energy cutoff component was removed. Residuals of the best fit LMC X-4 spectra with the four above mentioned models showed some line like features around 1 and 2 keV. Therefore, while fitting the LMC X-4 spectrum we included two gaussian components.

Similar to SMC X-1, the phase averaged spectrum could be fitted well with all the four models described above and the parameter values for the best fit obtained for each model are given in Table 3. The photon index (Γ_1) of the hard power-law component is identical in all the four models, ~ 0.70 . A black-body for the soft component requires a temperature of 0.17 keV and for a distance of 55 kpc of the LMC, if the black-body emission region is assumed to be spherical, it should have a radius of ~ 300 km. In Figure 9, the SIS and GIS count rate spectra are shown along with the components of model-I in the upper panel, while the residuals to the best fit model are shown in the bottom panel. A thermal bremsstrahlung emission with a temperature of 0.5 keV and emission measure of $5 \times 10^{60} \text{ cm}^{-3}$ also fits the soft excess well. If the soft excess is modeled in the form of an additional power-law, it has a photon index of 2.9, whereas an inversely broken power law type spectrum requires a soft photon index of ~ 1.9 below a break energy of 1.7 keV. Compared to the broken power-law model, the two power-law model, which has a cross-over energy of 1.5 keV, gives a steeper soft power-law. In addition, there are line-like features at ~ 1.0 and ~ 1.9 keV which we tentatively identify as iron L_α and Si_{XII} . The width of these two low energy lines were fixed at 0.1 keV during the spectral fit. The iron K_α line is centered at 6.4 keV and is broad (gaussian $\sigma = 0.65$ keV), with an equivalent width of 140 ± 40 eV. The L/K line ratio is model dependent, and is in the range of 2–5.

Woo et al. (1996) and La Barbera et al. (2001) fitted the soft excess in LMC X-4 as thermal bremsstrahlung emission. The temperature and flux of the thermal bremsstrahlung component obtained in Model II is similar to the their measurements, which were also carried out in high state of LMC X-4. Same is true about the flux and equivalent width of the iron emission line. La Barbera et al. (2001) found evidence of two distinct iron emission lines from the Beppo-SAX observation and the 6.1 keV line remains unexplained. However, an independent analysis of the same data (Oosterbroek et al. 2002, private communication) was found to favour a model consisting of a hard power-law, a black body type soft component, an emission line at 0.9 keV and a single iron emission line. The residuals of the best fitted model spectrum from the ROSAT and GINGA data (Figure 5 of Woo et al. 1996) also show the possibility of two weak emission lines at ~ 1 keV and ~ 2 keV.

3.2.3. *Pulse phase resolved spectrum*

Similar to the case with SMC X-1, only four parameters related to the shape and strength of the hard power-law and the soft excess were allowed to vary while all the other spectral parameters were fixed to their phase averaged value.

After the barycentric and orbital motion corrections of the photon arrival times, spectra were extracted from 16 uniformly divided pulse phases. All but the photon index and normalisation of the hard power-law component and temperature and normalisation of the soft component were fixed to their best fit values obtained from the pulse averaged spectrum. Modulations of flux from the hard and the soft components are shown in Figure 10 along with the total flux. The phase resolved spectra show that the power-law component follows the high-energy (> 1.5 keV) pulse profile with three peaks and the soft component (either black-body or bremsstrahlung) is consistent to a single peaked sinusoidal modulation similar to the pulse profile in the soft band (< 1.5 keV). For the SIS0 spectra in the FAST mode, background subtraction was not done, area discrimination was used to select the source photons, and hot and flickering pixels were not removed whose effect is relatively small in this mode. Due to these effects, the spectral parameters obtained from analysis of the SIS0 data are inaccurate. However, the pulse phase dependence of the spectral components derived from the SIS0 data are still reliable and agrees well with the results obtained from the GIS data.

Though the pulse phase variation of the black-body flux of LMC X-4 is consistent with a sinusoidal nature, a very low pulse fraction in this source and relatively large error bars makes it far from conclusive. Since the pulse profile of LMC X-4 in higher energy band shows several narrow features, a coarse phase bin in LMC X-4 will not show any variation in the high energy band. We, therefore, only show the flux of the black-body component obtained from four equal phase bins in the bottom panel of Figure 10. Since the statistics is poor in LMC X-4, a comparison similar to what is presented in Figure 6 for SMC X-1, could not be made.

4. Discussion

The pulse phase averaged spectra of these two accretion powered bright X-ray pulsars obtained with ASCA clearly show the presence of a soft component, which is in excess of the hard power-law component extended to lower energies. The present work is a confirmation of the presence of soft excess in LMC X-4 and SMC X-1. Pulse phase resolved spectroscopy, presented here, clearly show that in SMC X-1, the soft component when fitted by a black-

body (or thermal bremsstrahlung) model, exhibits a sinusoidal pulse shape regardless of the complex, sharp profile in hard energy band. The same may also be true for LMC X-4. A dissimilar pulse profile between the low and high energy bands is an indication that the soft component may have a different origin of emission, or at least the geometry of emission is different in different energy ranges. In LMC X-4, La Barbera et al. (2001) also fitted the soft excess as seed photon emission from accretion disk at magnetospheric radius Comptonized by moderately hot electrons. We have verified that this model can fit the soft excess seen in the ASCA spectra of both SMC X-1 and LMC X-4 with electron temperature of ~ 1.0 keV and optical depth of 8–10. If the soft photons are produced from the vicinity of the Alfvén radius, a modulation of the soft excess at the pulse period is difficult to explain.

Among the other X-ray pulsars known to have soft excess, in which pulse phase resolved spectroscopy has also been done, RX J0059.2–7138 (Kohno et al. 2000) and X Per (Coburn et al. 2001) do not show any modulation in the soft component, XTE 0111.2–7317 shows a pulse modulation of soft excess which is approximately in phase with the power-law component (Yokogawa et al. 2000b), and Her X-1 shows a pulse modulation of soft excess which has a different phase of pulse peak compared to the power-law component (Endo et al. 2000). The luminosity in the soft X-ray excess in SMC X-1 and LMC X-4 are 8.4×10^{36} and 7.7×10^{36} erg s $^{-1}$ respectively, a factor of 7–8 larger compared to that of Her X-1. In Her X-1, the soft excess, which is modeled as a black-body type emission, probably comes from a part of the X-ray irradiated inner accretion disk (Endo et al. 2000). In addition to the soft component, there is also a broad low energy emission line with a pulse shape and phase identical with that of the black-body emission. The total amount of X-ray emission in the soft excess is 1.1×10^{36} erg s $^{-1}$, which is 10% of the total emission in the ASCA energy band. In comparison with Her X-1, the ratio of the black-body flux to the total flux, is somewhat smaller in SMC X-1 (3.6%) and LMC X-4 (6.4%). In many ways, SMC X-1 and LMC X-4 are quite similar to Her X-1. It is interesting to investigate whether the presence of the soft component and its pulsating nature can be explained in a manner similar to Her X-1.

The soft excess can be a part of the X-ray emission from regions close to the neutron star reprocessed by optically thick surrounding matter in the inner accretion disk. With an assumption that the phase averaged pulsar emission is isotropic, the reprocessing region holds a solid angle that is equal to the fraction of X-ray energy reprocessed ($\sim 5\%$ in SMC X-1 and LMC X-4). From energy conservation, the radius at which the reprocessing region is situated (r_{BB}), presumably the inner accretion disk or Alfvén radius, can be calculated from the expression

$$\frac{L_X}{4\pi r_{\text{BB}}^2} = \sigma T^4,$$

where L_X is the total X-ray luminosity and T is the temperature of the black-body emission.

For SMC X-1 ($L_X = 2.4 \times 10^{38}$ erg s $^{-1}$) and LMC X-4 ($L_X = 1.2 \times 10^{38}$ erg s $^{-1}$), r_{BB} is calculated to be 12×10^7 cm and 9.4×10^7 cm respectively.

Here, we make a comparison of Alfvén radius (r_A) in these two pulsars with the same in Her X-1. For a given mass and radius of the neutron star, the inner radius scales as $r_A \propto B^{\frac{4}{7}} L_X^{-\frac{2}{7}}$. In these two pulsars, L_X is larger by about one order of magnitude than that in Her X-1. The magnetic field strength (B) in SMC X-1 is unknown, but the spectral cutoff energy indicate that B is smaller than that in Her X-1 (Makishima et al. 1999). In LMC X-4, a spectral cutoff at 16 keV and a recently discovered cyclotron absorption feature at ~ 100 keV with the Beppo-SAX (La Barbera et al. 2001) are in disagreement with the correlation observed in other accretion powered X-ray pulsars. However, considering L_X and B (corresponding to the Beppo-SAX measurement of the cyclotron absorption feature), the radius of the inner accretion disk is expected to be smaller in these two pulsars compared to Her X-1. On the contrary, in Her X-1, r_{BB} is found to be 3.6×10^7 cm (Endo et al. 2000), somewhat smaller than r_{BB} estimated above for SMC X-1 and LMC X-4. This is one reason we suspect that a black-body type emission cannot satisfactorily explain the soft excess in these two bright X-ray pulsars.

However, absence of convincing direct measurement of the magnetic field strength in these two pulsars result in some ambiguity in the Alfvén radius. We also note that X-ray irradiated inner accretion disk can be highly ionised with color temperature higher than the effective temperature. Presence of weak undetected emission lines may also cause the energy spectrum to deviate from a perfect blackbody, and the estimated parameters for the black-body emission region may include large systematic errors. Considering the above factors, we feel that it may still be possible to interpret that the Alfvén radius is the emission site of the black-body type soft excess.

Regarding Model II for the spectrum, a large emission measure (5×10^{61} and 7×10^{60} cm $^{-3}$ for SMC X-1 and LMC X-4 respectively) required for the soft excess indicates that with a thin thermal condition ($\tau \leq 1.0$), the emission region has to be extremely large ($\gtrsim 5 \times 10^{12}$ cm and $\gtrsim 8 \times 10^{11}$ cm for SMC X-1 and LMC X-4 respectively). Since the light travel time across such a region is much larger than the pulse periods in consideration, a pulsating soft component can not be produced by such a plasma. Moreover, even at extremely high densities, the cooling time scale of the plasma will be larger than the pulse periods of these pulsars. A pulsating nature of the soft component, therefore, cannot be explained in the thermal bremsstrahlung model also.

The two alternate models for the pulsar spectrum that we have tried here give somewhat satisfactory fit to the observed spectra. An additional soft power-law or an inversely broken shape of the power-law may also arise naturally when the entire emission is from the accretion

column. The distribution of temperature and matter density in the accretion column and transparency of radiation of different energy to the magnetic field structure determines the pulse profile and the energy spectrum. The soft component probably arises from upper part of the accretion column while the hard component is from the lower part. The different pulse shape and pulse phases of the soft and hard spectral components in Her X-1 have been compared with the model emission from an accretion mound on the magnetic pole of a neutron star (Burnard, Arons, and Klein 1991). Different types of beaming at different energy bands and at different heights of the accretion column can give rise to the observed energy dependence of the pulse profiles. The high, near-Eddington luminosity of SMC X-1 and LMC X-4, most of which is in the hard power-law component can be explained in a fan beam type emission pattern, in which the X-ray emission is perpendicular to the matter flow in the accretion columns. Observations of these type of bright pulsars in future, with instruments having better energy resolution and sensitivity in the lower energy band may help us to find an exact model of the pulsar spectrum.

5. Conclusions

In the present work we have found that these two high luminosity pulsars show pulsations in the entire energy band of 0.5–10.0 keV, with strong energy dependence in the pulse shape. The pulse phase averaged energy spectra definitely show the presence of soft excess in both the sources. If the soft excess is modeled as a separate black-body or thermal bremsstrahlung type component, pulse phase resolved spectroscopy shows that the soft component has a pulsating nature in SMC X-1, which may also be true for LMC X-4. We have found that the pulse profile of the soft component is nearly sinusoidal, significantly different from the sharp, complex profile of the hard power-law component. Due to very high luminosity of these sources, the size of the emission zone required for the soft component is large (radius \sim 300–400 km) and we find that it is difficult to explain the pulsations detected at low energies. We have found that alternate models like inversely broken power-law or two different power-law components can also be used to describe the spectra.

We thank R. Sunyaev and A. R. Rao for some useful discussions. This research has made use of data obtained through the High Energy Astrophysics Science Archive Research Center Online Service, provided by the NASA/Goddard Space Flight Center. B. Paul was supported by the Japan Society for the Promotion of Science through a fellowship during which most of this work was done. FN acknowledges the support by the Japan Science and Technology Corporation under the ACT-JST project.

REFERENCES

- Burnard, D. J., Arons, J., & Klein, R. I. 1991, 367, 575
- Coburn, W., Heindl, W. A., Gruber, D. E., Rothschild, R. E., Staubert, R., Wilms, J., & Kreykenbohm, I. 2001, ApJ(in press) astro-ph/0101110
- Dal Fiume, D., Orlandini, M., Cusumano, G., del Sordo, S., Feroci, M., Frontera, F., Oosterbroek, T., Palazzi, E., Parmar, A. N., Santangelo, A., & Segreto, A. 1998, A&A, 329, L41
- Dennerl, K., 1989, in "Two Topics in X Ray Astronomy", 23rd ESLAB Symposium, vol. 1 : X-ray Binaries, p39
- Endo, T., Nagase, F., & Mihara, T. 2000, PASJ, 52,223
- Kohno, M., Yokogawa, J., & Koyama, K. 2000, PASJ, 52,299
- La Barbera, A. , Burderi, T., Di Salvo, T., Iaria, R., & Robba, N. R. 2001, astro-ph/0104367
- Lang, F. L., Levine, A. M., Bautz, M., Hauskins, S., Howe, S., Primini, F. A., Lewin, W. H. G., Baity, W. A., Knight, F. K., Rotschild, R. E., & Petterson, J. A. 1981, ApJ, 246, L21
- Levine, A. M., Rappaport, S. A., & Zojcheski, G. 2000, ApJ, 541, 194
- McCray, R. A., Shull, J. M., Boynton, P. E., Deeter, J. E., Holt, S. S., & White, N. E. 1982, ApJ, 262, 301
- Makishima, K., Mihara, T., Nagase, F., & Tanaka, Y. 1999, ApJ, 525, 978
- Marshall, F. E., Becker, R. H., & White, N. E. 1983, ApJ, 266, 814
- Morrison, R., & McCammon, D. 1983, ApJ, 270, 119
- Oosterbroek, T., Parmar, A. N., Dal Fiume, D., Orlandini, M., Santangelo, A., Del Sordo, S., & Segreto, A. 2000, A&A, 353, 575
- Oosterbroek, T., Parmar, A. N., Martin, D. D. E., & Lammers, U. 1997, A&A, 327, 215
- Orlandini, M., Fiume, D. D., Frontera, F., Del Sordo, S., Piraino, S., Santangelo, A., Segreto, A., Oosterbroek, T., & Parmar, A. N. 1998, ApJ, 500, L163
- Tanaka, Y., Inoue, H., & Holt, S. S. 1994, PASJ, 46, L37

- Vrtilek, S. D., Boroson, B., Cheng, F. H., McCray, R., & Nagase, F. 1997 *ApJ*, 490, 377
- White, N. E., Nagase, F., & Parmar, A. N. 1995, in "X-ray Binaries", eds. W. H. G. Lewin, J. van Paradijs & E. P. J. van den Heuvel (Cambridge University Press: Cambridge),
- Wojdowski, P., Clark, G. W., Levine, A. M., Woo, J. W., & Zhang, S. N. 1998, *ApJ*, 502, 253
- Woo, J. W., Clark, G. W., Blondin, J. M., Kallman, T. R., & Nagase, F. 1995, *ApJ*, 445, 896
- Woo, J. W., Clark, G. W., Levine, A. M., Corbet, R. H. D., & Nagase, F. 1996, *ApJ*, 467, 811
- Yokogawa, J., Imanishi, K., Tsujimoto, M., Nishiuchi, M., Koyama, K., Nagase, F., & Corbet, R. H. D. 2000a, *ApJS*, 128, 491
- Yokogawa, J., Paul, B., Ozaki, M., Nagase, F., Chakrabarty, D., & Takeshima, T. 2000b, *ApJ*, 539, 191

Table 1. The spectral parameters of SMC X-1

Parameter	Model I	Model II	Model III	Model IV
N_H^a	2.16 ± 0.32	3.52 ± 0.31	2.10 ± 0.22	5.3 ± 0.5
Photon index (Γ_1)	0.91 ± 0.03	0.93 ± 0.04	0.95 ± 0.02	0.87 ± 0.04
Power-law norm(I_{PL}) ^b	2.98 ± 0.12	3.13 ± 0.16	5.18 ± 0.22	2.9 ± 0.2
Break energy (keV)	–	–	1.68 ± 0.04	–
Photon index (Γ_2)	–	–	1.90 ± 0.10	4.85 ± 0.30
Power-law norm(I_{PLs}) ^b	–	–	–	8.3 ± 1.2
BB/BR temp (keV)	0.179 ± 0.009	0.33 ± 0.03	–	–
BB/BR norm ^c	6750^{+2000}_{-2500}	0.46 ± 0.20	–	–
Cutoff Energy (E_C) keV	$5.5^{+1.4}_{-0.5}$	$6.3^{+0.9}_{-2.0}$	$5.5^{+2.8}_{-0.7}$	5.7 ± 1.1
E-folding energy (E_F) keV	35^{+23}_{-20}	25^{+25}_{-10}	55 ± 40	25 ± 15
Fe Line centre energy (keV)	6.32 ± 0.16	$6.31^{+0.17}_{-0.22}$	6.32 (fixed)	$6.41^{+0.17}_{-0.13}$
Fe Line width (keV)	0.5 ± 0.2	$0.5^{+0.3}_{-0.2}$	0.50 (fixed)	0.42 ± 0.22
Fe Line norm ^d	$8.3^{+6.5}_{-4.7}$	9.5 ± 6.5	$9.5^{+1.7}_{-2.5}$	$6.1^{+4.0}_{-3.5}$
Reduced χ^2 /dof	0.961/477	1.03/477	1.18/479	1.22/477

^a 10^{21} atoms cm^{-2}

^b 10^{-2} photons $\text{cm}^{-2} \text{s}^{-1} \text{keV}^{-1}$ at 1 keV

^c BB: $\left(\frac{R_{\text{km}}}{D_{10 \text{ kpc}}}\right)^2$; BR: $\frac{3.2 \times 10^{-60}}{4\pi D_{10 \text{ kpc}}^2} \int n_e n_1 dV \text{ cm}^{-3}$

^d 10^{-4} photons $\text{cm}^{-2} \text{s}^{-1}$

Table 2. Pulse phase resolved spectral parameters of SMC X-1 for Model I

Parameter	Main pulse	1st minima	Sub pulse	2nd minima
N_{H}^{a}	6.0 ± 0.6	4.6 ± 1.2	7.9 ± 1.7	3.9 ± 1.9
Photon index (Γ_1)	1.13 ± 0.02	1.09 ± 0.06	1.10 ± 0.07	1.05 ± 0.08
Power-law norm(I_{PL}) ^b	2.05 ± 0.07	1.16 ± 0.11	1.55 ± 0.16	1.03 ± 0.13
BB temp (keV)	0.135 ± 0.004	0.142 ± 0.012	0.133 ± 0.009	0.149 ± 0.017
BB flux ^c (0.7-10.0 keV)	1.14	0.81	0.84	0.67
BB flux (% of total flux in 0.7-10.0 keV)	5.0	5.9	4.9	5.1
Reduced χ^2/dof	1.16/599	0.92/304	1.00/306	0.87/245

^a 10^{21} atoms cm^{-2}

^b 10^{-2} photons $\text{cm}^{-2} \text{s}^{-1} \text{keV}^{-1}$ at 1 keV

^c 10^{-11} erg $\text{cm}^{-2} \text{s}^{-1}$

Table 3. The spectral parameters of LMC X-4

Parameter	Model I	Model II	Model III	Model IV
N_{H}^{a}	$5.7^{+3.8}_{-0.0}$	$5.7^{+3.2}_{-0.0}$	$5.7^{+1.3}_{-0.0}$	$5.7^{+5.5}_{-0.0}$
Photon index (Γ_1)	0.69 ± 0.04	0.75 ± 0.05	0.73 ± 0.03	0.59 ± 0.04
Power-law norm(I_{PL}) ^b	1.48 ± 0.07	1.41 ± 0.10	2.66 ± 0.06	1.07 ± 0.08
Break energy (keV)	–	–	1.75 ± 0.04	–
Photon index (Γ_2)	–	–	1.94 ± 0.07	$2.9^{+0.7}_{-0.2}$
Power-law norm(I_{PLS}) ^b	–	–	–	1.3 ± 0.3
BB/BR temp (keV)	$0.170^{+0.12}_{-0.18}$	0.51 ± 0.04	–	–
BB/BR norm ^c	4660^{+4100}_{-1100}	$0.053^{+0.025}_{-0.007}$	–	–
L1 Line centre energy (keV)	0.96 ± 0.04	0.93 ± 0.03	0.95 ± 0.03	0.90 ± 0.03
L1 Line norm ^d	19 ± 4	35 ± 9	21 ± 5	56 ± 13
L2 Line centre energy (keV)	1.93 ± 0.04	1.94 ± 0.05	1.88 ± 0.03	1.93 ± 0.05
L2 Line norm ^d	3.0 ± 0.7	1.6 ± 0.6	4.0 ± 0.8	1.1 ± 0.6
Fe Line centre energy (keV)	6.47 ± 0.12	6.49 ± 0.11	$6.56^{+0.18}_{-0.12}$	6.44 ± 0.12
Fe Line width (keV)	0.52 ± 0.15	0.57 ± 0.15	0.68 ± 0.20	0.55 ± 0.15
Fe Line norm ^d	6.5 ± 2.0	7.4 ± 2.1	10 ± 4	7.0 ± 2.0
Reduced χ^2/dof	1.38/340	1.37/339	1.35/340	1.31/339

^a 10^{20} atoms cm^{-2}

^b 10^{-2} photons $\text{cm}^{-2} \text{s}^{-1} \text{keV}^{-1}$ at 1 keV

^c BB: $\left(\frac{R_{\text{km}}}{D_{10 \text{ kpc}}}\right)^2$; BR: $\frac{3.2 \times 10^{-60}}{4\pi D_{10 \text{ kpc}}^2} \int n_e n_{\text{I}} dV \text{ cm}^{-3}$

^d 10^{-4} photons $\text{cm}^{-2} \text{s}^{-1}$

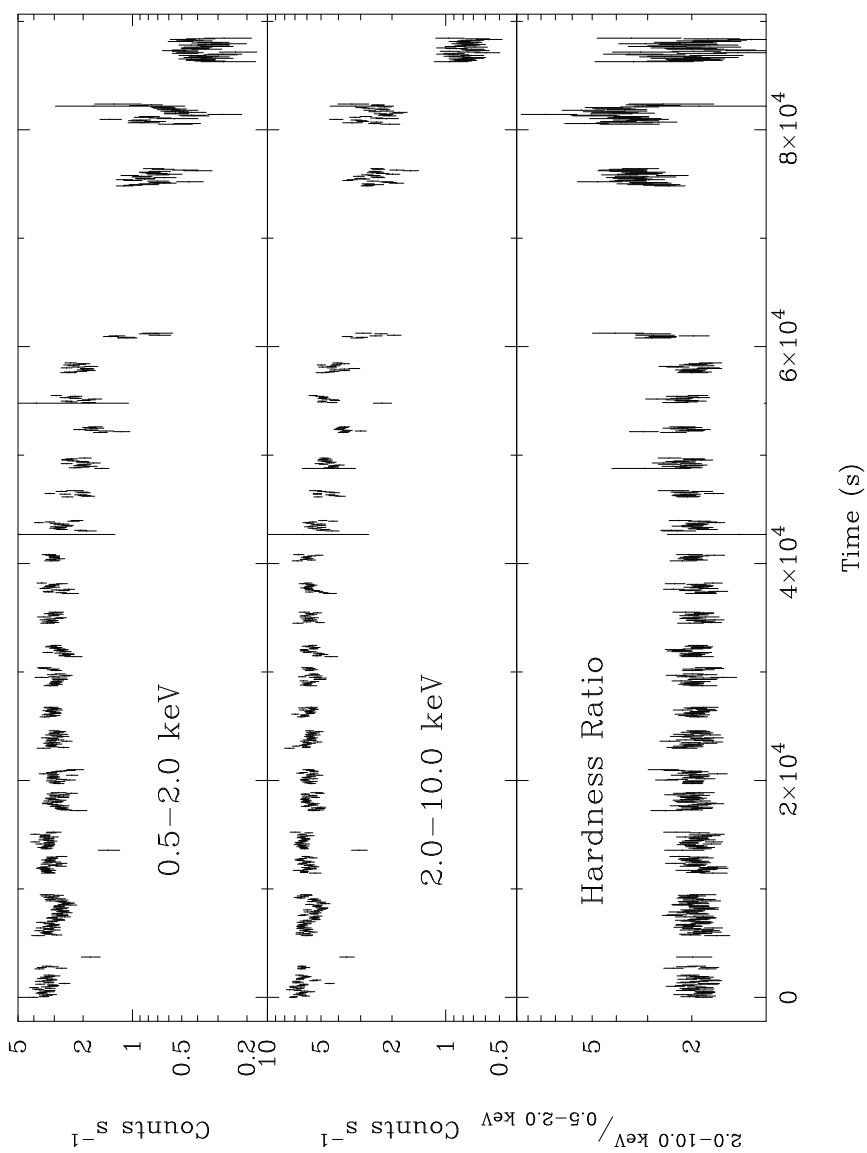


Fig. 1.— The light curves of SMC X-1 in two energy bands of 0.5–2.0 and 2.0–10.0 keV and the hardness ratio obtained from the GIS data of the 1993 observation are shown here. Spectral changes can be noticed near the end of the observation. For the spectral analysis

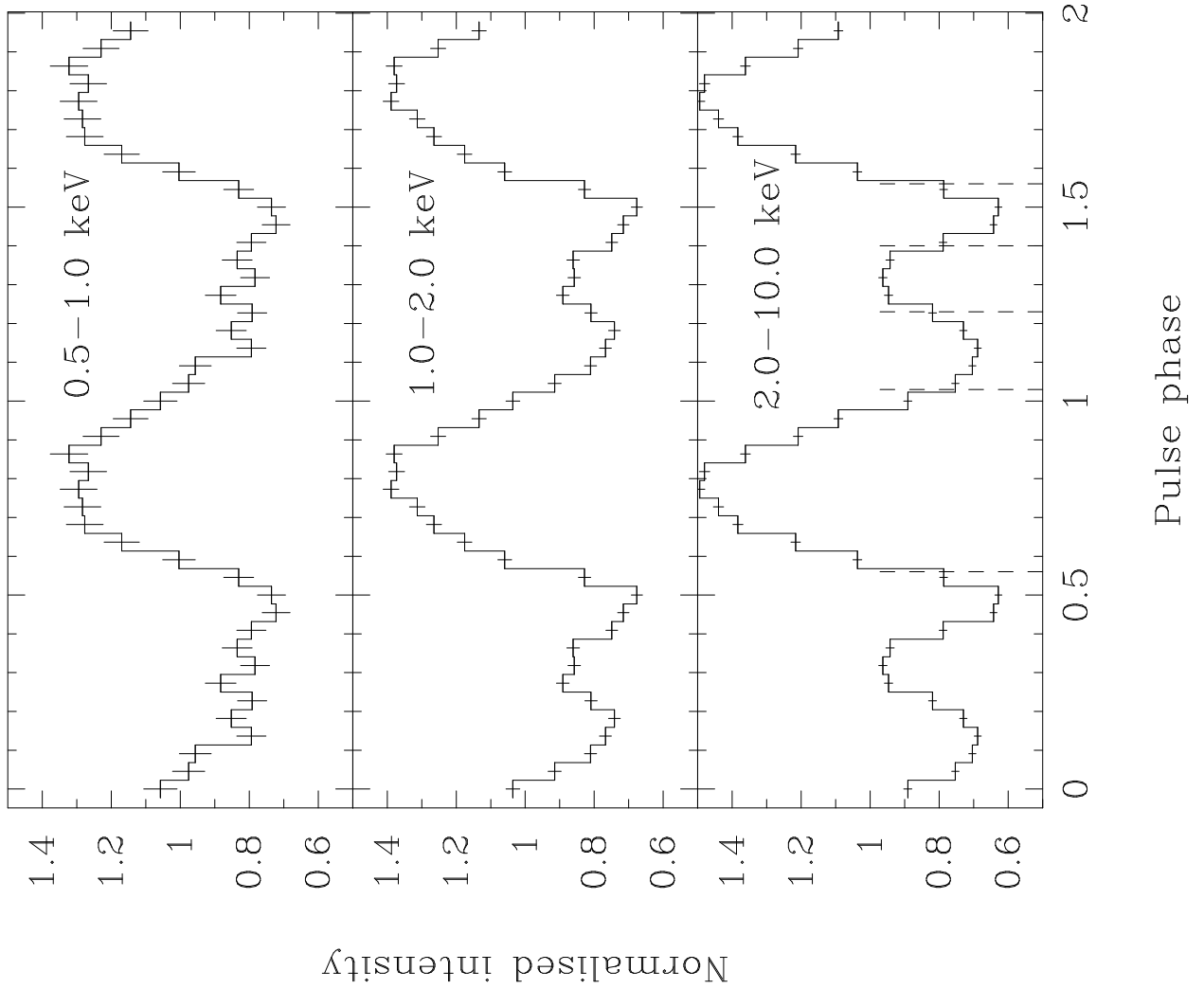


Fig. 2.— The normalised pulse profiles of SMC X-1 in three energy bands obtained with the GIS in the 1993 observation are plotted here. The main peak, sub peak and the two minima regions chosen for coarse phase resolved spectroscopy are marked in the bottom panel.

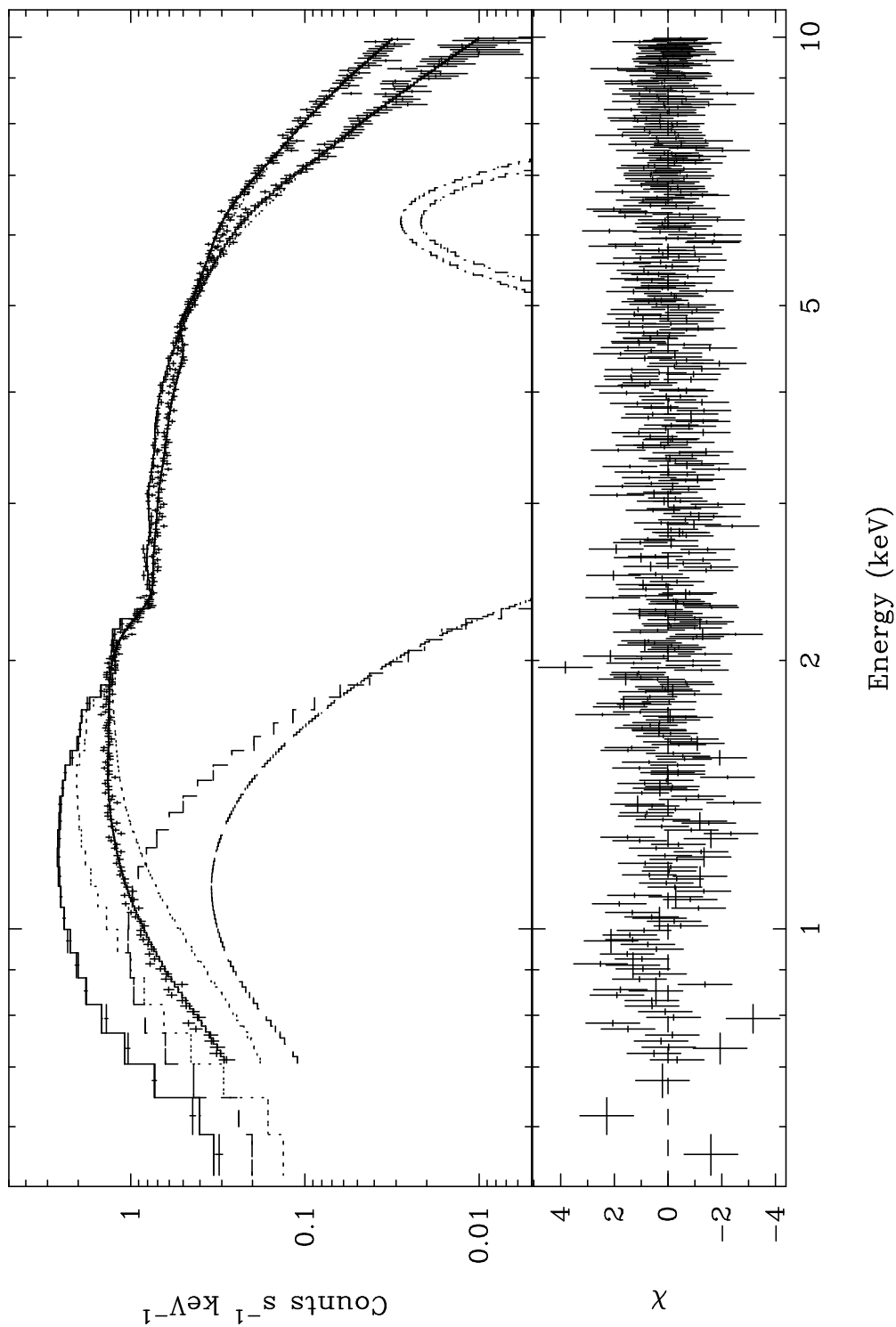


Fig. 3.— The energy spectra of SMC X-1 obtained with the SIS and GIS are shown here along with the best fit model comprising three components, an exponentially cutoff power-law, a broad iron line emission, and a soft black-body emission. The lower panel shows the contributions of the residuals to the χ^2 for each energy bin.

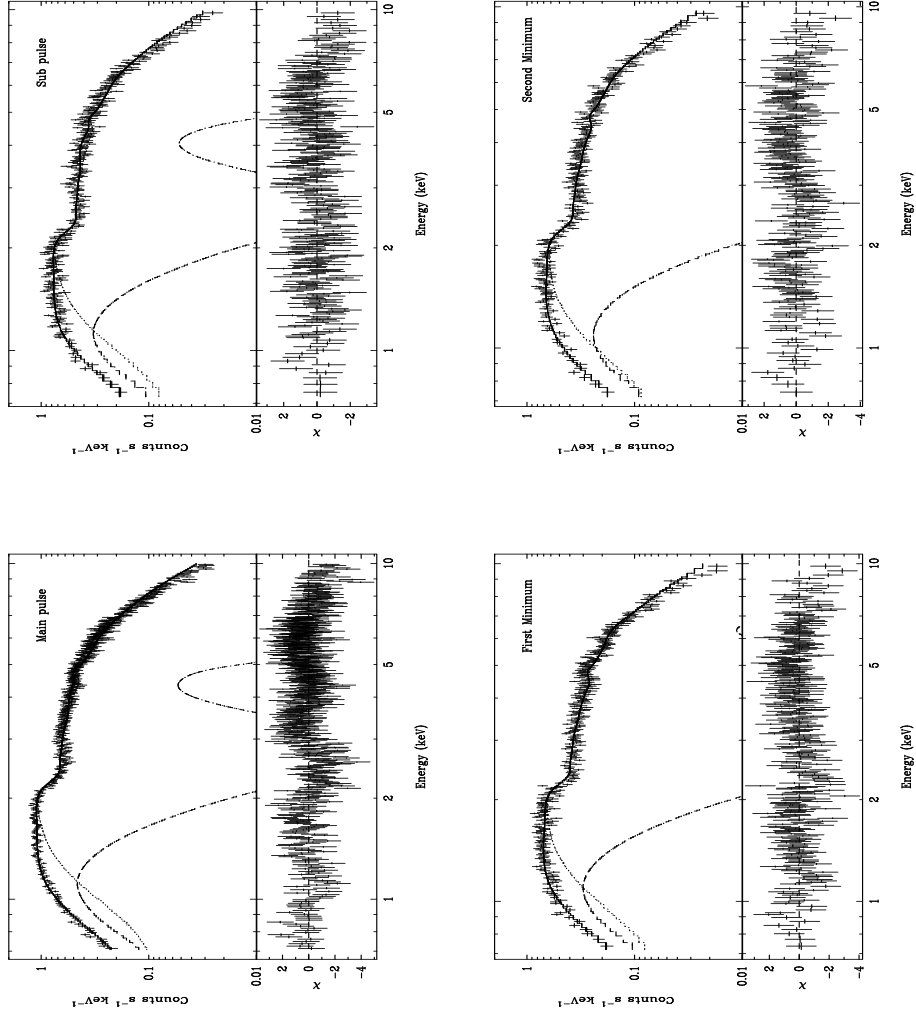


Fig. 4.— Phase resolved spectra of SMC X-1 obtained with ASCA-GIS.

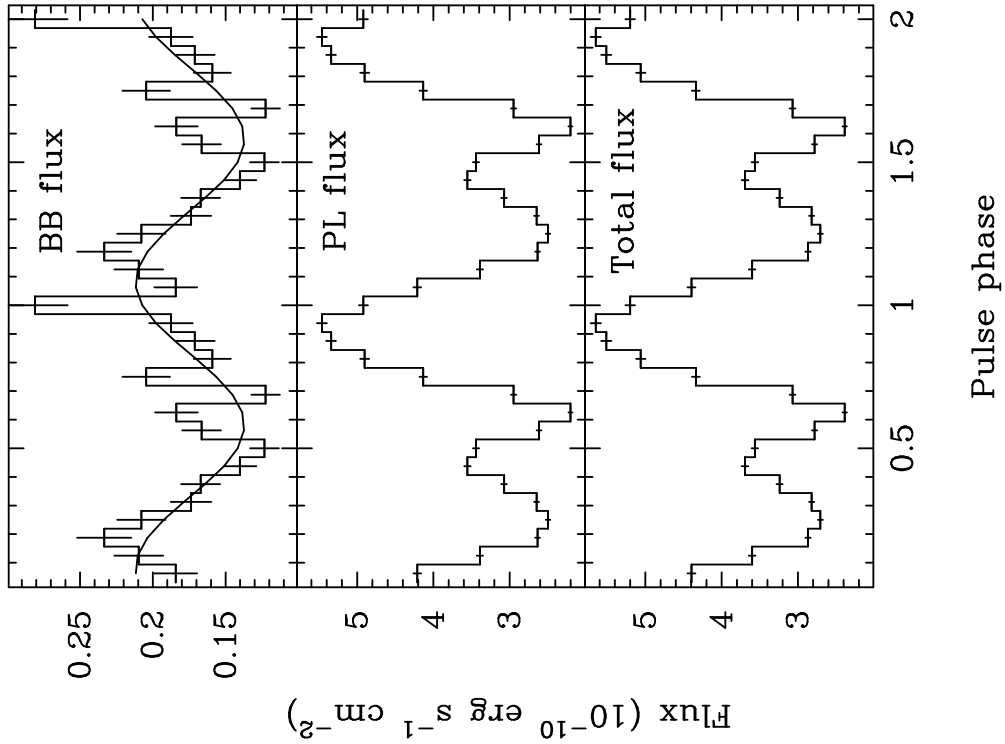


Fig. 5.— Modulation of the black-body flux, power-law flux, and total flux in the 0.5–10.0 keV band of SMC X-1 obtained from pulse phase resolved analysis of the GIS spectrum with Model I are shown here for two cycles. With Model II, the bremsstrahlung component was found to have pulsations similar to the black-body component shown here. The curve in the top panel is the best fit sinusoidal, given here to indicate the almost sinusoidal nature of the soft excess modulation.

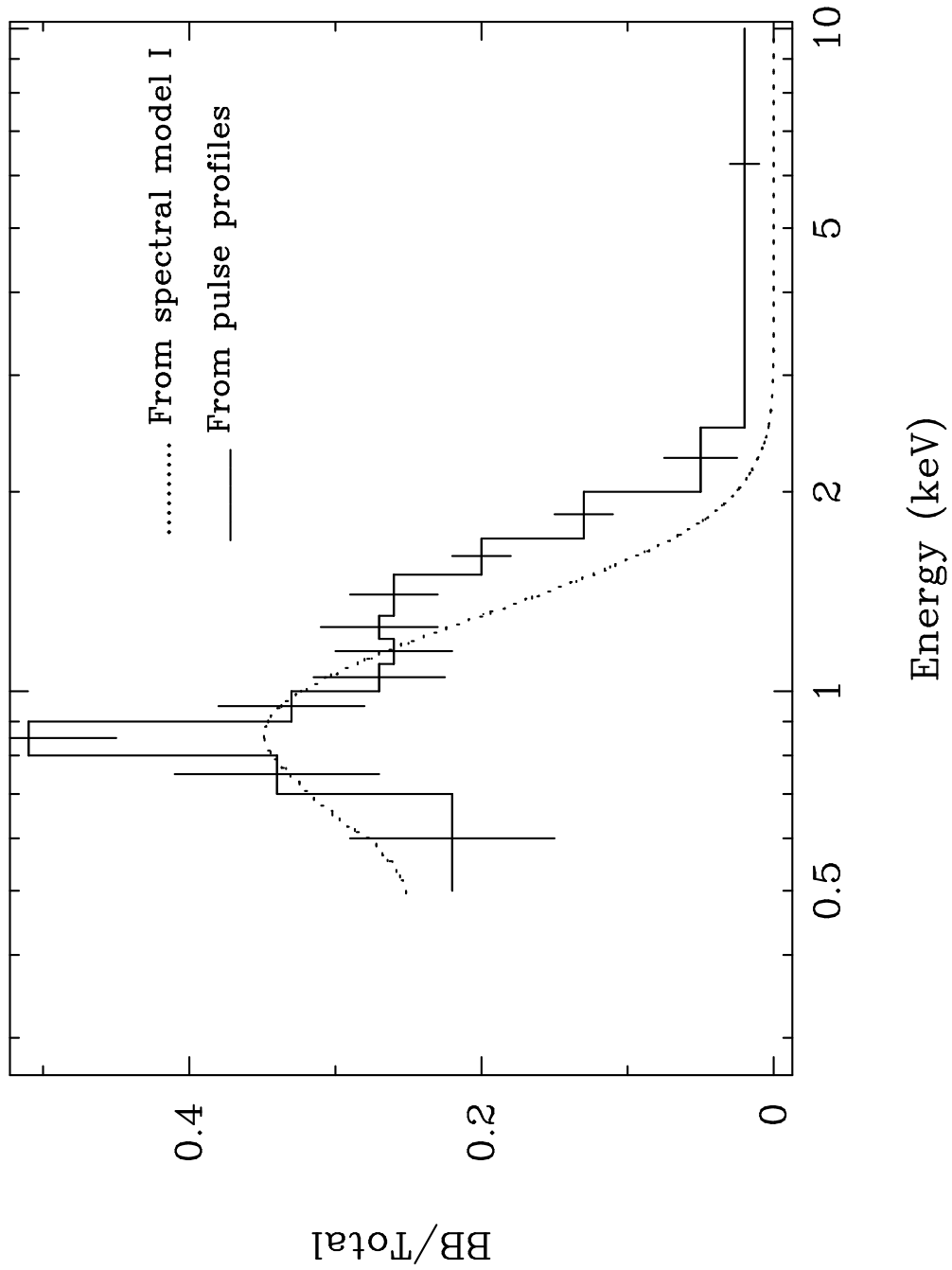


Fig. 6.— Ratio of the black-body to total flux from the spectral model is compared with the fraction of sinusoidal (black-body) component in the SMC X-1 pulse profile at different energies

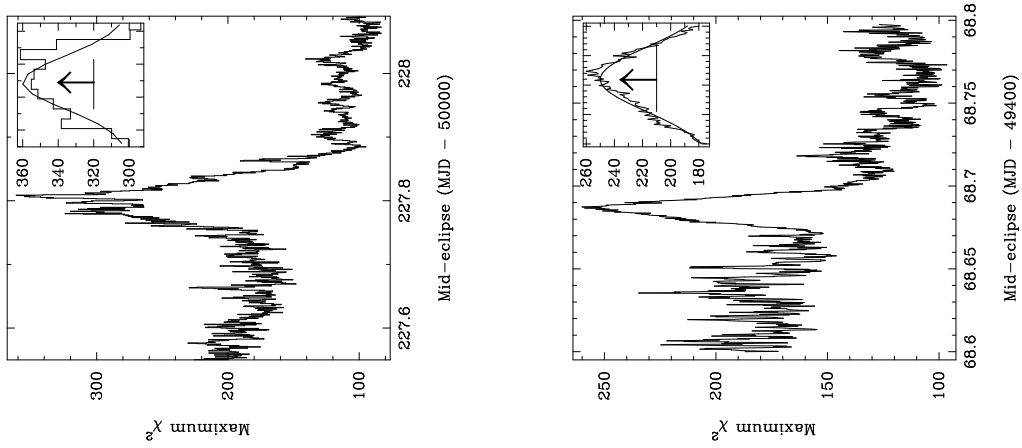


Fig. 7.— The maximum χ^2 obtained from pulse folding technique is plotted here against the trial mid-eclipse epochs for the 1994 and 1996 ASCA observations of LMC X-4. Expanded view of the region of interest is shown in the inset of each panel. The center and width of the best fitted gaussians are marked with arrow and horizontal line.

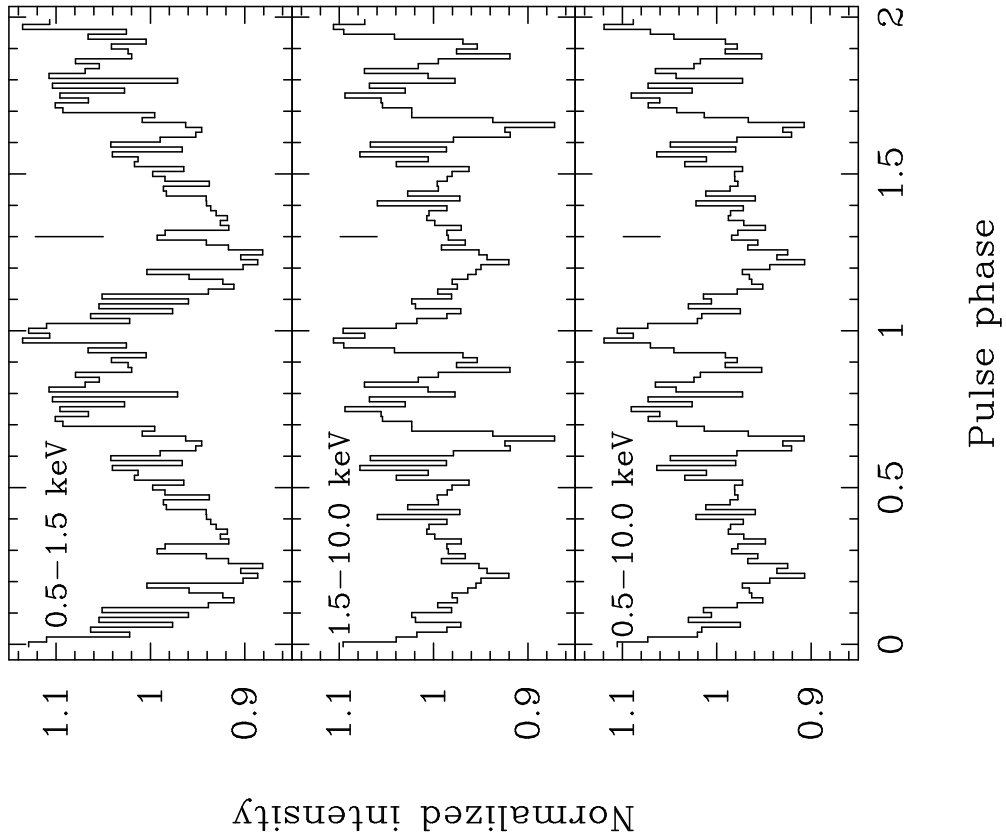


Fig. 8.— The normalised pulse profiles of LMC X-4 in three energy bands obtained with the ASCA-GIS are shown here. Typical error bars are given in each panel.

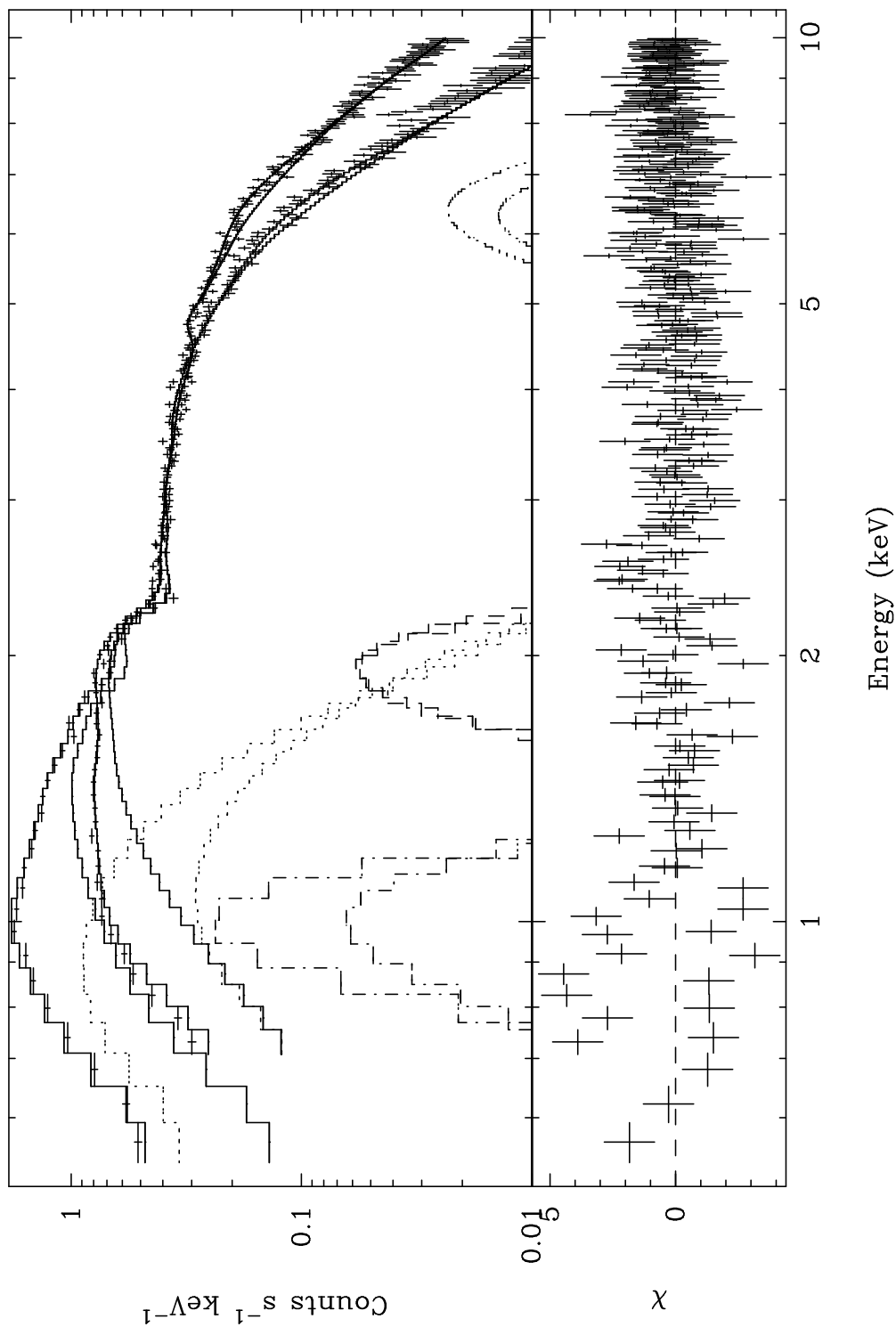


Fig. 9.— The energy spectra of LMC X-4 obtained with the SIS1 and two GIS detectors are shown here along with the best fit model comprising an absorbed power-law, a broad iron line emission, a soft black-body emission and two low energy emission lines. The lower panel shows the contributions of the residuals to the χ^2 for each energy bin.

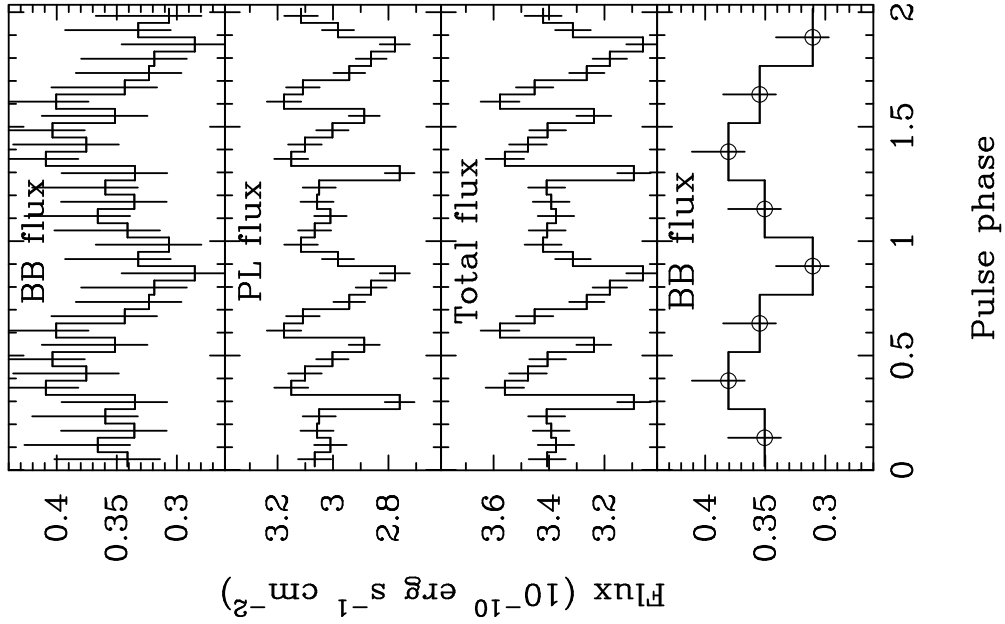


Fig. 10.— Modulation of the black-body flux, power-law flux, and total flux in the 0.5–10.0 keV band obtained from pulse phase resolved analysis of GIS spectrum of LMC X-4 with Model I are shown in the top three panels for two cycles. With Model II, the bremsstrahlung component was found to have pulsations similar to the black-body component shown here. Variation of the black body flux, obtained from a coarse phase binning is shown in the bottom panel.